



## Shear viscosity of an ultracold Fermi gas in the BCS-BEC crossover

Jing Min(闵靖), Xiangchuan Yan(严祥传), Da-Li Sun(孙大立), Lu Wang(王璐), Xin Xie(谢馨), Xizhi Wu(吴熙至), Shi-Guo Peng(彭世国), and Kaijun Jiang(江开军)

**Citation:** Chin. Phys. B, 2025, 34 (5): 053103. DOI: 10.1088/1674-1056/adc403

<http://cpb.iphy.ac.cn>; <https://iopscience.iop.org/cpb>

### What follows is a list of articles you may be interested in

---

## Effect of conical intersection of benzene on non-adiabatic dynamics

Duo-Duo Li(李多多) and Song Zhang(张嵩)

Chin. Phys. B, 2022, 31 (8): 083103. DOI: 10.1088/1674-1056/ac5607

## Effects of pressure and gas-jet thickness on the generation of attosecond pulse

Li Xiao-Yong (李小勇), Wang Guo-Li (王国利), Zhou Xiao-Xin (周效信)

Chin. Phys. B, 2014, 23 (1): 013102. DOI: 10.1088/1674-1056/23/1/013102

## Time-dependent density functional theoretical studies on the photo-induced dynamics of an HCl molecule encapsulated in C<sub>60</sub> under femtosecond laser pulses

Liu Dan-Dan (刘丹丹), Zhang Hong (张红)

Chin. Phys. B, 2013, 22 (10): 103103. DOI: 10.1088/1674-1056/22/10/103103

## Effect of electron correlation on high-order harmonic generation in helium model atom

Hu Shi-Lin (胡师林), Shi Ting-Yun (史庭云)

Chin. Phys. B, 2013, 22 (1): 013101. DOI: 10.1088/1674-1056/22/1/013101

---

# Shear viscosity of an ultracold Fermi gas in the BCS–BEC crossover

Jing Min(闵靖)<sup>1,2</sup>, Xiangchuan Yan(严祥传)<sup>1</sup>, Da-Li Sun(孙大立)<sup>1,†</sup>, Lu Wang(王璐)<sup>1,2</sup>, Xin Xie(谢馨)<sup>1,2</sup>,  
Xizhi Wu(吴熙至)<sup>1,2</sup>, Shi-Guo Peng(彭世国)<sup>1</sup>, and Kaijun Jiang(江开军)<sup>1,3,‡</sup>

<sup>1</sup>State Key Laboratory of Magnetic Resonance and Atomic and Molecular Physics,  
Innovation Academy for Precision Measurement Science and Technology, Chinese Academy of Sciences, Wuhan 430071, China

<sup>2</sup>University of Chinese Academy of Sciences, Beijing 100049, China

<sup>3</sup>Wuhan Institute of Quantum Technology, Wuhan 430206, China

(Received 31 December 2024; revised manuscript received 21 March 2025; accepted manuscript online 24 March 2025)

We report on the measurement of shear viscosity in an ultracold Fermi gas with variable temperatures and tunable interactions. A quadrupole mode excitation in an isotropic harmonic trap is used to quantify the shear viscosity of the quantum gas within the hydrodynamic regime. The shear viscosity of the system as a function of temperature has been investigated, and the results closely align with calculations in the high-temperature limit utilizing a new definition of the cutoff radius. Through an adiabatic sweep across the Bardeen–Cooper–Schrieffer (BCS) to Bose–Einstein condensate (BEC) crossover, we find that the minimum value of the shear viscosity, as a function of interaction strength, is significantly shifted toward the BEC side. Furthermore, the behavior of the shear viscosity is asymmetric on both sides of the location of the minimum.

**Keywords:** shear viscosity, quadrupole mode, hydrodynamic theory, BCS–BEC crossover

**PACS:** 31.70.Hq, 34.20.+x, 37.10.Jk

**DOI:** 10.1088/1674-1056/adc403

**CSTR:** 32038.14.CPB.adc403

## 1. Introduction

Ultracold Fermi gases<sup>[1,2]</sup> offer an exceptional platform for systematically investigating the physical properties of strongly correlated quantum systems through the application of Feshbach resonance.<sup>[3]</sup> Recently, the study of shear viscosity ( $\eta$ ) in ultracold Fermi gases has garnered significant interest.<sup>[4–11]</sup> During the transport process, shear viscosity plays a crucial role in determining the damping or dissipation behavior, providing valuable insights into the transport properties of quantum systems.

Beyond its significance as a hydrodynamic quantity, shear viscosity has captivated researchers due to the Kovtun–Son–Starinets (KSS) bound,<sup>[12]</sup> which posits that the ratio of shear viscosity to entropy density ( $\eta/s$ ) in any fluid is constrained by the inequality  $\eta/s \geq \hbar/(4\pi k_B)$ . Notably, the observed  $\eta/s$  in a <sup>6</sup>Li unitary Fermi gas exceeds this lower bound by approximately 5 times,<sup>[5,13]</sup> a value comparable to that found in quark-gluon plasmas.<sup>[14]</sup> Furthermore, it has been reported that the shear viscosity  $\eta$  reaches a minimum value slightly on the BEC side,<sup>[15]</sup> rather than at the unitarity limit under the same energy scale. This motivates us to experimentally measure  $\eta$  during the adiabatic variation of interaction strength in an isentropic process.

Numerous experimental methods have been developed to measure the shear viscosity, including radial breathing

mode,<sup>[5]</sup> anisotropic expansion,<sup>[11,15]</sup> and the fitting of density perturbations in a homogeneous system.<sup>[16]</sup> However, the experimental data across different measurements vary substantially. Additionally, establishing a reliable theoretical model in the regime of strong interactions remains challenging. In summary, the behavior of shear viscosity in a strongly interacting Fermi gas has not yet been fully characterized, particularly in the BCS–BEC crossover region.

In this work, we excite the quadrupole mode (the superposition of  $(l, m) = (2, 2)$  and  $(l, m) = (2, -2)$ )<sup>[17–19]</sup> in a spherical Fermi gas<sup>[20]</sup> to extract the system’s shear viscosity from the damping rate of the oscillation. Here,  $l$  is the orbital angular momentum quantum number and  $m$  is the magnetic quantum number, ranging from  $-l$  to  $+l$ . The  $m = 2$  and  $m = -2$  represent counter-rotating quadrupole in the  $x$ – $y$  plane, perpendicular to the trap’s axial direction ( $z$ -axis), and their superposition results in a standing wave-like oscillation. Due to the small ratio of the collisional mean free path to the cloud size (Knudsen number  $k_n = (0.023 \sim 0.038) \ll 1$ )<sup>[15]</sup> in our system, it operates in the hydrodynamic limit across a wide temperature range. Notably, the excited quadrupole mode does not oscillate along the  $z$ -axis and exhibits out-of-phase oscillations in the  $x$ - and  $y$ -directions. This characteristic effectively suppresses the impact of bulk viscosity on the oscillations, enabling more precise shear viscosity measure-

<sup>†</sup>Corresponding author. E-mail: dlsun@wipm.ac.cn

<sup>‡</sup>Corresponding author. E-mail: kjjiang@wipm.ac.cn

© 2025 Chinese Physical Society and IOP Publishing Ltd. All rights, including for text and data mining, AI training, and similar technologies, are reserved.

<http://iopscience.iop.org/cpb> <http://cpb.iphy.ac.cn>

ments across the crossover region. Using this methodology, we assess the temperature dependence of shear viscosity in the unitary regime. Furthermore, by adiabatically tuning the interaction of atoms,<sup>[21]</sup> we investigate the evolution of shear viscosity across the BCS–BEC crossover region.

## 2. Hydrodynamic theory

### 2.1. The trap-averaged shear viscosity coefficient

The collective oscillation of a unitary Fermi gas can be considered in the framework of hydrodynamic theory, with the continuity equation<sup>[5,20,22]</sup>

$$\frac{\partial n}{\partial t} + \nabla \cdot (n\mathbf{v}) = 0 \quad (1)$$

and the Navier–Stokes equation

$$m \left[ n \frac{\partial}{\partial t} + n(\mathbf{v} \cdot \nabla) \right] v_i = - \frac{\partial p}{\partial r_i} + \sum_j \frac{\partial}{\partial r_j} (\eta \sigma_{ij} + \zeta_b \sigma' \delta_{ij}) - n \frac{\partial V_{\text{ext}}}{\partial r_i}, \quad (2)$$

where  $n(\mathbf{r}, t)$  is the density,  $\mathbf{v}(\mathbf{r}, t)$  is the velocity field,  $p(\mathbf{r}, t)$  is the local pressure,  $V_{\text{ext}}(\mathbf{r}, t)$  is the external potential,  $\eta$  is the shear viscosity,  $\zeta_b$  is the bulk viscosity,  $\sigma_{ij} = \partial v_i / \partial x_j + \partial v_j / \partial x_i - 2\delta_{ij} \nabla \cdot \mathbf{v} / 3$ , and  $\sigma' = \nabla \cdot \mathbf{v}$ .

Considering the evolution of the atomic cloud size defined as  $\langle r_i^2 \rangle = \int d\mathbf{r} r_i^2 n(\mathbf{r}, t) / N$ , we obtain

$$\frac{d^2 \langle r_i^2 \rangle}{dt^2} \frac{1}{2} = \frac{1}{mN} \int p d\mathbf{r} + \langle v_i^2 \rangle - \frac{1}{m} \left\langle r_i \frac{\partial V_{\text{ext}}}{\partial r_i} \right\rangle - \frac{\hbar}{m} \langle \alpha_s \sigma_{ii} + \alpha_b \sigma' \rangle, \quad (3)$$

where we have defined the shear viscosity  $\eta = \alpha_s \hbar n$ , bulk viscosity  $\zeta_b = \alpha_b \hbar n$ , and  $\langle f \rangle = \int d\mathbf{r} f n(\mathbf{r}, t) / N$ . To solve the hydrodynamic equation, we adopt an ansatz for the density profile at time  $t$

$$n(x, y, z, t) = \frac{1}{b_x b_y b_z} n_0 \left( \frac{x}{b_x}, \frac{y}{b_y}, \frac{z}{b_z} \right), \quad (4)$$

where  $n_0(\mathbf{r})$  is the initial density profile,  $b_i$  is the scaling factor, and the corresponding velocity field  $\mathbf{v}(\mathbf{r}, t)$  is fixed by the continuity equation  $v_i(\mathbf{r}, t) = \dot{b}_i(t) r_i / b_i(t)$ .

For a Fermi gas in an isotropic harmonic trap with arbitrary interaction strength, we assume that the equation of state follows a power law  $\mu(n) \propto n^\gamma$ ,<sup>[1,20,23,24]</sup> where  $n$  is the average atomic density and  $\gamma$  is the effective exponent that depends on the interaction strength. With the form  $b_i^2(t) = \langle r_i^2 \rangle(t) / \langle r_i^2 \rangle_0$  and  $\mu(n)$ , we substitute those into Eqs. (3) and (4), ultimately obtaining the equation satisfied by  $b_i(t)$  as

$$\frac{\ddot{b}_i}{b_i} = \frac{\omega_i^2}{b_i^2 (b_x b_y b_z)^\gamma} - \omega_i^2 - \frac{\hbar \bar{\alpha}_s}{m \langle r_i^2 \rangle_0 b_i^2} \sigma_{ii} - \frac{\hbar \bar{\alpha}_b}{m \langle r_i^2 \rangle_0 b_i^2} \sigma', \quad (5)$$

where the trap-averaged shear (bulk) viscosity coefficient is defined as  $\bar{\alpha}_{s(b)} = N^{-1} \int d\mathbf{r} n \alpha_{s(b)}$ , and  $\langle r_i^2 \rangle_0$  is the mean square radius of atomic cloud in the trap along the  $i$ th axis before the excitation.

For a small quadrupole mode oscillation, Eq. (5) is linearized by  $b_i(t) \approx 1 + \varepsilon_i(t)$  ( $\varepsilon_i \ll 1$ ), and the oscillation occurs only in the  $x$ – $y$  plane but is out of phase between the oscillations along the  $x$  and  $y$  axes with an equal amplitude. Thus we have

$$\varepsilon_x(t) = -\varepsilon_y(t) = \varepsilon_\perp(t), \quad \varepsilon_z(t) = 0. \quad (6)$$

For a unitary Fermi gas, we have  $\alpha_b = 0$ ,<sup>[5,25–27]</sup> the fourth term on the right-hand side of Eq. (5) is zero. For a finite interaction strength, the bulk viscosity is not zero anymore ( $\alpha_b \neq 0$ ). Fortunately, spherical geometry suggests that the finite value of  $\alpha_b$  does not significantly affect the decay of quadrupole mode oscillations in comparison to shear viscosity. As

$$\sigma' = \frac{\dot{b}_x}{b_x} + \frac{\dot{b}_y}{b_y} + \frac{\dot{b}_z}{b_z} = \frac{\dot{\varepsilon}_\perp}{1 + \varepsilon_\perp} - \frac{\dot{\varepsilon}_\perp}{1 - \varepsilon_\perp} \approx -2\varepsilon_\perp \dot{\varepsilon}_\perp, \quad (7)$$

$$\sigma_{ii} = 2 \frac{\dot{b}_i}{b_i} - \frac{2}{3} \left( \frac{\dot{b}_x}{b_x} + \frac{\dot{b}_y}{b_y} + \frac{\dot{b}_z}{b_z} \right) \approx 2\dot{\varepsilon}_i, \quad (8)$$

where  $\dot{\varepsilon}_i \gg \varepsilon_i \dot{\varepsilon}_i$ . Then Eq. (5) yields

$$\frac{d^2 \varepsilon_\perp}{dt^2} + \frac{2\hbar \bar{\alpha}_s}{m \langle r_i^2 \rangle_0} \frac{d\varepsilon_\perp}{dt} + 2\omega_0^2 \varepsilon_\perp = 0. \quad (9)$$

Comparing the equation above with a standard damped harmonic oscillation equation  $d^2x/dt^2 + 2\Gamma dx/dt + \omega^2 x = 0$ , we can readily determine the frequency  $\omega_Q$  and the damping rate  $\Gamma_Q$  of the quadrupole mode oscillation as

$$\omega_Q = \sqrt{2}\omega_0, \quad (10)$$

$$\Gamma_Q = \frac{\hbar \bar{\alpha}_s}{m \langle r_i^2 \rangle_0}. \quad (11)$$

The value of the mean square radius  $\langle r_i^2 \rangle_0$  for a unitary Fermi gas can be calculated as  $\langle r_i^2 \rangle_0 = \langle r_i^2 \rangle(t_{\text{TOF}}) / (1 + \omega_0^2 t_{\text{TOF}}^2)$ . While with the finite interactions, we operate under the assumption that  $3\gamma E_{\text{rel}} = 2U_{\text{trap}}$ ,<sup>[1,20,23,24]</sup> where  $E_{\text{rel}}$  is the release energy during the process of free expansion. We can determine the value of  $\langle r_i^2 \rangle_0$  using the expression  $U_{\text{trap}} = 3\gamma E_{\text{rel}} / 2 = \sum_i m \omega_0^2 (\langle r_i^2 \rangle_0) / 2$ . Here,  $\gamma$  is calculated using zero-temperature theory,<sup>[23]</sup> and  $E_{\text{rel}}$  is determined from experiments involving long-time free expansion.<sup>[20]</sup>

The shear viscosity can be measured by exciting other vibrational modes of the system. When  $\sigma_{ii}$  in Eq. (5) is nonzero, the relationship between the damping rate and the shear viscosity can be established, which allows us to determine the shear viscosity. For example, consider the quadrupole mode

( $l = 2, m = 0$ ) in an isotropic harmonic trap with the variation amplitude  $\varepsilon_x(t) = \varepsilon_y(t) = -\varepsilon_z(t)/2$ , and the radial breathing mode in an axially symmetric harmonic trap with  $\varepsilon_x(t) = \varepsilon_y(t)$  and  $\varepsilon_z(t) = 0$ ,<sup>[28,29]</sup> both having a value of  $\sigma_{ii} \neq 0$ .

## 2.2. The cutoff radius

In general, the shear viscosity can be expressed as

$$\eta = \hbar n \alpha_s \left( \frac{T}{T_F(n)}, k_F(n)a, k_F(n)R \right), \quad (12)$$

where  $T_F(n)$  ( $k_F(n)$ ) is the local Fermi temperature (wave vector),  $n$  is the atomic density,  $\alpha_s$  is the local shear viscosity coefficient which is a function of the equation of state. Here, the shear viscosity's dependences of the s-wave scattering length  $a$  and effective range  $R$  are included. In the high-temperature limit, one can obtain the exact result

$$\begin{aligned} & \alpha_s \left( \frac{T}{T_F(n)}, k_F(n)a, k_F(n)R \right) \\ &= \frac{\alpha_{3/2}}{2} \left( \frac{T}{T_F} \right)^{3/2} I^{-1} \left( \frac{T}{T_F(n)}, k_F(n)a, k_F(n)R \right), \end{aligned} \quad (13)$$

where  $\alpha_{3/2} = 45\pi^{3/2}/64\sqrt{2}$ . The integral  $I$  is given by

$$\begin{aligned} & I \left( \frac{T}{T_F(n)}, k_F(n)a, k_F(n)R \right) \\ &= \int_0^\infty dx e^{-x} x^3 \left[ \frac{2T_F(n)}{T} \left( \frac{1}{k_F(n)a} + \frac{x k_F(n)RT}{T_F(n)} \right)^2 + x \right]^{-1}. \end{aligned} \quad (14)$$

Let us neglect the effective range correction for the moment. At resonance, we obtain the result

$$\begin{aligned} & \alpha_s \left( \frac{T}{T_F(n)}, k_F(n)a \rightarrow \infty, 0 \right) \\ &= \alpha_{3/2} \left( \frac{T}{T_F(n)} \right)^{3/2} \approx 2.77 \left( \frac{T}{T_F(n)} \right)^{3/2}, \end{aligned} \quad (15)$$

the same result as those obtained in Refs. [30–33].

Then we calculate the trap-averaged shear viscosity

$$\bar{\alpha}_s = \frac{\alpha_{3/2} \theta_0^{3/2}}{N} \int_0^{R_c} dr n(r) \left( \frac{\theta}{\theta_0} \right)^{3/2}, \quad (16)$$

where  $R_c$  represents the cutoff radius in the integral, which is introduced to account for the breakdown of hydrodynamics in the outer regions of the cloud. In these outer regions, the particle mean free paths become too long, violating the fundamental assumption of hydrodynamic theory.<sup>[34]</sup>  $\theta \equiv T/T_F(n)$  is the local reduced temperature, and  $\theta_0 \equiv T/T_F(n_0)$  is the reduced temperature at the trap center. At high temperature, the atomic density is well fitted by a Gaussian function,  $n(r) = n_0 \exp(-r^2/\sigma^2)$ , where  $n_0 = N/(\sqrt{\pi}\sigma)^3$  is the

density at the trap center. The mean square radius is evaluated as  $\langle r^2 \rangle_0 = 3 \langle r_i^2 \rangle_0 = 3\sigma_i^2/2$  for  $i = x, y, z$ , and thus we have  $n_0 = N(2\pi \langle r^2 \rangle_0/3)^{-3/2} = N(2\pi \langle r_i^2 \rangle_0)^{-3/2}$ . Since  $(\theta/\theta_0)^{3/2} = [T_F(n_0)/T_F(n)]^{3/2} = n_0/n$ , it gives

$$\bar{\alpha}_s = \frac{4\pi\alpha_{3/2}}{3N} \theta_0^{3/2} n_0 R_c^3 = \frac{\sqrt{6}\alpha_{3/2}\theta_0^{3/2}}{\sqrt{\pi}} \frac{R_c^3}{\langle r^2 \rangle_0^{3/2}}, \quad (17)$$

$$\theta_0 = \frac{4}{3\pi^{1/3}} \frac{E}{E_F} \frac{T}{T_F}. \quad (18)$$

If  $R_c = \langle r^2 \rangle_0^{1/2}$ , we have

$$\bar{\alpha}_s = \frac{\sqrt{6}\alpha_{3/2}}{\sqrt{\pi}} \theta_0^{3/2}. \quad (19)$$

We can also fit the Gaussian distribution using a Thomas–Fermi function and obtain the effective Thomas–Fermi radius  $R_{TF} \approx 1.25 \sqrt{\langle r^2 \rangle_0}$ . Setting  $R_c = R_{TF}$ , we get

$$\bar{\alpha}_s = \frac{\sqrt{6}\alpha_{3/2} 1.25^3}{\sqrt{\pi}} \theta_0^{3/2}. \quad (20)$$

## 3. Experimental results

In our experiment,  ${}^6\text{Li}$  atoms with two balanced spin states  $|F = 1/2, m_F = \pm 1/2\rangle$  are trapped in an isotropic harmonic trap. We prepare a spherical degenerate Fermi gas of  ${}^6\text{Li}$  with the atom number of  $N = 3.6 \times 10^4$  and temperature of  $T/T_F = 0.29$ , following our previous work.<sup>[20,35,36]</sup> To mitigate the anharmonic effect of the trap, we gradually increase the optical intensity to a high value over approximately 70 ms, then maintain stability for 10 ms to allow the system to reach equilibrium. The geometric mean trapping frequency is  $\omega_0 = (\omega_x \omega_y \omega_z)^{1/3} = 2\pi \times 1131$  Hz. The corresponding asphericity is  $\delta = (\omega_{\max} - \omega_{\min})/\omega_0 \approx 4.9\%$ , where  $\omega_{\max}$  and  $\omega_{\min}$  are the maximum and minimum frequencies along three axes, respectively.

To excite the quadrupole mode oscillation, which is a superposition of two oscillation modes with  $l = 2, m = -2$  and  $l = 2, m = +2$ , we apply a sinusoidal asymmetric modulation to the trap in the  $x$ – $y$  plane for 4 periods, with  $\omega_x^2(t) = \omega_x^2 [1 + \beta \sin(\Omega_Q t)]$  and  $\omega_y^2(t) = \omega_y^2 [1 - \beta \sin(\Omega_Q t)]$ , where  $\beta = 0.045$  is the excitation amplitude and the modulation frequency is  $\Omega_Q = \sqrt{2}\omega_0$ . The atomic cloud oscillates out of phase along the  $x$  and  $y$ -axes, while the size along the  $z$ -axis remains nearly constant. After varying the holding time  $t$  in the trap, the atomic cloud is imaged in the  $x$ – $y$  plane with a time of flight (TOF) of  $t_{\text{TOF}} = 1$  ms. The mean square radius of the atomic cloud in an arbitrary direction,  $\langle r_i^2 \rangle(t + t_{\text{TOF}})$ , is obtained by fitting a Gaussian distribution to the atomic density profile. The quadrupole mode oscillation can be described by

$$A_Q = \frac{\langle r_x^2 \rangle(t + t_{\text{TOF}}) - \langle r_y^2 \rangle(t + t_{\text{TOF}})}{\langle \langle r_x^2 \rangle \rangle(t + t_{\text{TOF}}) + \langle \langle r_y^2 \rangle \rangle(t + t_{\text{TOF}})}, \quad (21)$$

where  $\langle\langle r_x^2 \rangle\rangle(t + t_{\text{TOF}}) + \langle\langle r_y^2 \rangle\rangle(t + t_{\text{TOF}})$  is the average value of each data set. As shown in Fig. 1, the quadrupole mode is excited at different temperatures in the unitary regime, and the oscillation is fitted with a damped sinusoidal function  $A_Q = \delta A_Q \sin(\omega_Q t + \phi) \exp(-\Gamma_Q t)$ . In order to observe the trend of the quadrupole mode oscillation as a function of temperature  $T/T_F$ , we vary the trap depth at the end of the evaporative cooling process. Ultimately, the temperature  $T/T_F$  is changed from 0.29 to 0.44. Figure 1 displays the temperatures from top to bottom, which are  $T/T_F = 0.29, 0.34$  and  $0.38$ , respectively. The fitting frequencies of the quadrupole mode oscillation are  $\omega_Q = 2\pi \times [1648(22), 1671(28), 1621(34)]$  Hz, all of which are approximately  $\sqrt{2}\omega_0$ , consistent with the prediction from hydrodynamic theory. As the initial temperature of the atomic cloud increases, the damping rate of the quadrupole mode oscillation gradually rises, with values of  $\Gamma_Q = 503(28) \text{ s}^{-1}, 561(33) \text{ s}^{-1}$  and  $630(37) \text{ s}^{-1}$  respectively.

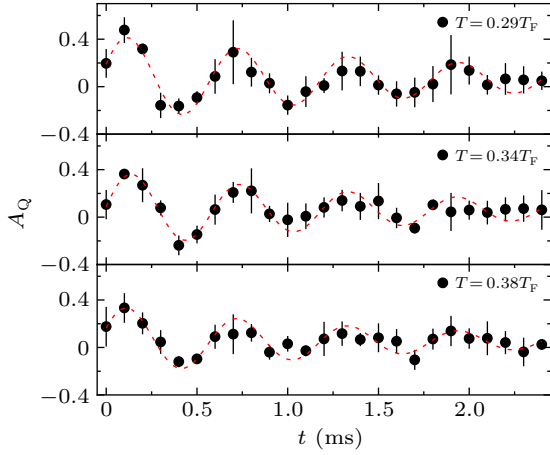


**Fig. 1.** Quadrupole mode of a unitary Fermi gas at different temperatures. Quadrupole mode oscillation as a function of the holding time  $t$  for different cloud temperatures. From top to bottom, the corresponding temperatures are  $T/T_F = 0.29, 0.34$  and  $0.38$ . The dashed lines represent the results of fitting the experimental data with a damped sinusoidal function.

By calculating in Eq. (11), the trap-averaged shear viscosity coefficient  $\bar{\alpha}_s$  can be derived from  $\Gamma_Q$ , as illustrated in Fig. 2. The value of  $\theta_0$  is calculated by using Eq. (18), where the total energy is  $E = m\omega_0^2 \langle r^2 \rangle_0$ ,<sup>[39]</sup> the Fermi energy is  $E_F = \hbar\omega_0 (3N)^{1/3}$  and the value of  $T/T_F$  can be determined by  $E/E_F$ .<sup>[40]</sup> Relevant shear viscosity coefficients measured in other groups are also displayed together.<sup>[5,11,37,38]</sup> Although there are discrepancies between different works, all the measurements show the same variation trend that  $\bar{\alpha}_s$  increases with temperature. From Subsection 2.2, if the cutoff radius is equal to the radius of the Gaussian distribution,  $R_c = \sqrt{\langle r^2 \rangle_0}$ , the calculation seems to provide a lower bound of the shear viscosity (black solid line in Fig. 2). We can also fit the Gaussian distribution using a Thomas–Fermi function and take the correctional Thomas–Fermi radius as the cutoff radius,  $R_c = R_{\text{TF}} \approx 1.25\sqrt{\langle r^2 \rangle_0}$ , and remarkably, it agrees well with our measurements (red solid line in Fig. 2). The values

of  $\bar{\alpha}_s$  obtained in Ref. [11] by expanding the atomic cloud lie below our and others' measurements<sup>[5,37,38]</sup> by exciting atoms in the trap.

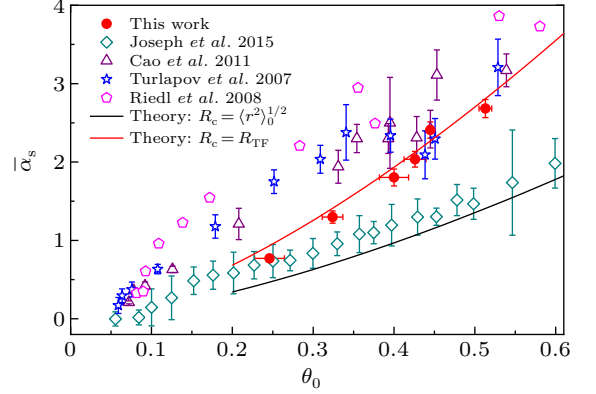


**Fig. 2.** Shear viscosity versus the temperature. The trap-averaged shear viscosity coefficient  $\bar{\alpha}_s$  increases with the reduced temperature  $\theta_0 = T/T_F(n_0)$ , where  $T_F(n_0)$  is the Fermi temperature with the central atomic density  $n_0$  in the trap. As a comparison of our results (red circles), the measured  $\bar{\alpha}_s$  from other groups are also listed, including Riedl *et al.*<sup>[37]</sup> (magenta pentagons), Turlapov *et al.*<sup>[38]</sup> (blue stars), Cao *et al.*<sup>[5]</sup> (purple triangles) and Joseph *et al.*<sup>[11]</sup> (darkcyan diamonds). The black solid line is the high-temperature calculation with the radius of the Gaussian distribution as the cutoff radius,  $R_c = \sqrt{\langle r^2 \rangle_0}$ , and the red solid curve with the correctional Thomas–Fermi radius as the cutoff radius,  $R_c = R_{\text{TF}} \approx 1.25\sqrt{\langle r^2 \rangle_0}$ . Both calculations are plotted above the superfluid transition with  $\theta_0 \geq 0.2$ .

Then, we measure the variation in shear viscosity as a function of interaction strength by performing an adiabatic sweep of the Feshbach magnetic field, starting from 832 G, across the BCS–BEC crossover regime. The entropy is conserved throughout this adiabatic sweep. Here the trapping frequency is  $\omega_0 = 2\pi \times 720$  Hz, the temperature is  $T/T_F = 0.26$  and the total atom number is  $N = 9.6 \times 10^4$  at 832 G. The adiabaticity was ensured through preliminary tests, in which we varied the magnetic field from 832 G to the BEC or BCS regimes and back at different ramp speeds. We monitor changes in cloud size to assess heating and excitation. For ramp speeds of 0.6 G/ms and lower, no oscillations or size increases were detected. Consequently, we maintain a constant ramp time of 450 ms to reach the target magnetic field. To measure the shear viscosity in the BCS–BEC crossover regime, we use quench dynamics to excite the quadrupole mode, following the method in Ref. [41]. First, we individually vary the trapping frequencies  $\omega_x$  (from  $2\pi \times 720$  Hz to  $2\pi \times 648$  Hz) and  $\omega_y$  (from  $2\pi \times 720$  Hz to  $2\pi \times 792$  Hz) over a 70 ms exponential ramp, and then we quench both frequencies back to  $2\pi \times 720$  Hz.

As the system moves away from resonance, the conformal symmetry is broken, and the bulk viscosity becomes nonzero. Fortunately, due to the spherical geometry, bulk viscosity effects are suppressed and negligible in our experiment (see Subsection 2.1).

Typical data sets of quadrupole mode oscillations at different interaction strengths are presented in Fig. 3. The os-

cillation frequency  $\omega_Q$  and damping rate  $\Gamma_Q$  are obtained by fitting the experimental data across the BCS–BEC crossover. The trapping frequency  $\omega_0$  is measured using the sloshing mode. The fitted oscillation frequencies consistently show  $\omega_Q = 2\pi \times [1020(20), 1018(8), 1039(6), 1054(20)]$  Hz with the interaction strength  $1/(k_F a) = -0.41$  ( $B = 920$  G), 0 ( $B = 832$  G), 0.29 ( $B = 790$  G) and 0.93 ( $B = 730$  G) respectively. All of these oscillation frequencies are approximately  $\sqrt{2}\omega_0$ , indicating that the system predominantly remains in the hydrodynamic regime. The corresponding decay rate  $\Gamma_Q = 1287(99) \text{ s}^{-1}$ ,  $348(33) \text{ s}^{-1}$ ,  $270(25) \text{ s}^{-1}$ , and  $1213(86) \text{ s}^{-1}$ . Notably, the quadrupole mode oscillation exhibits the smallest damping rate in the region near the resonance point on the BEC side.

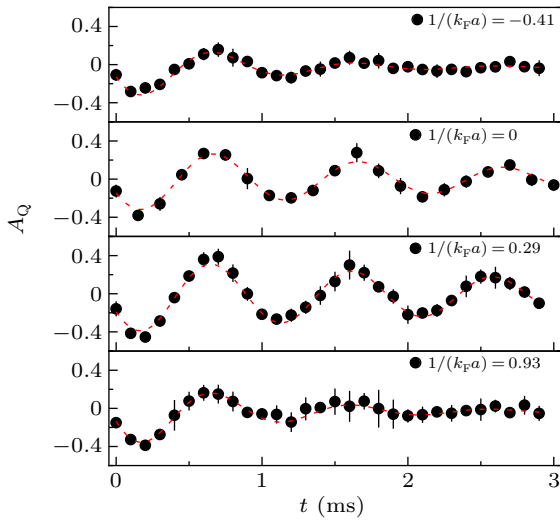


**Fig. 3.** Quadrupole mode of a Fermi gas for various interaction strengths. Quadrupole mode oscillation as a function of the holding time  $t$  at different interactions. The oscillation behaviors are represented for BCS ( $1/(k_F a) = -0.41$ ), unitary ( $1/(k_F a) = 0$ ) and BEC ( $1/(k_F a) = 0.29, 0.93$ ) regions, respectively. The dashed lines denote the results of fitting our data with a damped sinusoidal function.

Figure 4 shows the difference  $\Delta\bar{\alpha}_s = \bar{\alpha}_s - \bar{\alpha}_{s0}$  between the  $\bar{\alpha}_s$ , determined at finite  $1/(k_F a)$ , and the resonant value  $\bar{\alpha}_{s0}$ . The interaction region is defined within the range of  $-0.45 < 1/(k_F a) < 1$  to ensure the applicability of hydrodynamic theory, which is determined by observed quadrupole mode oscillation frequency. We now discuss the behavior of  $\Delta\bar{\alpha}_s$  in different regions in more detail.

For  $1/(k_F a) < 0$ , the shear viscosity decreases as the system nears the unitary region, consistent with increasing collision rates in the two-body limit, where viscosity is inversely related to collision rates.

For  $1/(k_F a) > 0$ , the change in shear viscosity is not monotonic; it initially decreases and then increases. The shift of the minimum shear viscosity toward the BEC side can be attributed to the corresponding increase in the dimer fraction. This phenomenon causes the cross section to enlarge within a small range near the resonance, resulting in a decrease in shear viscosity. It is important to point out that the location

of the minimum will move toward resonance with increasing temperature.<sup>[15]</sup>

For  $-0.45 < 1/(k_F a) < 1$ , the data for the entire region indicate that the change in shear viscosity is asymmetrical on both sides of the location of the minimum, which contrasts with the parabolic relationship observed in previous work.<sup>[15]</sup> Compared to the BEC side, the shear viscosity is larger on the BCS side. This behavior of shear viscosity has been analyzed through theoretical calculations that incorporate pairing fluctuations within the framework of a T-matrix approximation.<sup>[42]</sup> We utilize a third-order polynomial to fit the data, which reveals that the minimum point occurs at  $1/(k_F a) = 0.27$ . It is evident from the figure that the results of the parabolic fitting deviate significantly from the experimental data, highlighting a clear feature of asymmetry.

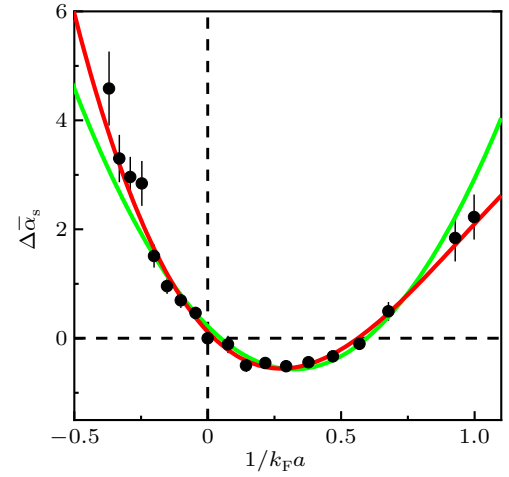


**Fig. 4.** Shear viscosity versus the interaction strength. The difference in trap-averaged shear viscosity coefficient on and off resonance,  $\Delta\bar{\alpha}_s$ , versus interaction strength  $1/(k_F a)$ , during the isentropic scanning of the magnetic field. The red curve represents the best fit of  $c_0 + c_1/(k_F a) + c_2/(k_F a)^2 + c_3/(k_F a)^3$  to the data with  $c_0 = 0.12$ ,  $c_1 = -5.2$ ,  $c_2 = 11.04$  and  $c_3 = -3.86$ . From the fit, the minimum of the shear viscosity occurs at  $1/(k_F a) = 0.27$ . For comparison, the green curve illustrates the results of fitting the data with a second-order polynomial.

## 4. Conclusions

In summary, we have measured the shear viscosity of the  ${}^6\text{Li}$  Fermi gas in the BCS–BEC crossover. We can determine the shear viscosity by exciting the quadrupole mode of the spherical Fermi gas and measuring the damping rate of the oscillation. This scheme allows the system to operate at the hydrodynamic limit across a wide range of temperatures while reducing the impact of bulk viscosity. The shear viscosity of the system as a function of temperature has been investigated, and the results closely align with calculations in the high-temperature limit using a new definition of the cut-off radius. Through an adiabatic sweep, we investigated the shear viscosity as a function of interaction strength  $1/(k_F a)$  and found that there is a minimum shear viscosity on the BEC side.<sup>[15]</sup> Furthermore, the asymmetric behavior of the shear

viscosity observed on both sides of the minimum location in the BCS–BEC crossover region differs from previous experimental findings, yet remains qualitatively consistent with recent theoretical results.

## Acknowledgments

Project supported by the National Key R&D Program (Grant No. 2022YFA1404102), the National Natural Science Foundation of China (Grant Nos. U23A2073, 12374250, and 12121004), Chinese Academy of Sciences (Grant No. YJKYYQ20170025), and Hubei Province (Grant No. 2021CFA027).

## References

- [1] Giorgini S, Pitaevskii L P and Stringari S 2008 *Rev. Mod. Phys.* **80** 1215
- [2] Bloch I, Dalibard J and Zwirger W 2008 *Rev. Mod. Phys.* **80** 885
- [3] Chin C, Grimm R, Julienne P and Tiesinga E 2010 *Rev. Mod. Phys.* **82** 1225
- [4] Rupak G and Schäfer T 2007 *Phys. Rev. A* **76** 053607
- [5] Cao C, Elliott E, Joseph J, Wu H, Petricka J, Schäfer T and Thomas J E 2011 *Science* **331** 58
- [6] Wlazłowski G, Magierski P and Drut J E 2012 *Phys. Rev. Lett.* **109** 020406
- [7] Guo H, Wulin D, Chien C C and Levin K 2011 *Phys. Rev. Lett.* **107** 020403
- [8] Bluhm M and Schaefer T 2016 *Phys. Rev. Lett.* **116** 115301
- [9] Bluhm M, Hou J and Schäfer T 2017 *Phys. Rev. Lett.* **119** 065302
- [10] Bruun G 2012 *Phys. Rev. A* **85** 013636
- [11] Joseph J, Elliott E and Thomas J 2015 *Phys. Rev. Lett.* **115** 020401
- [12] Kovtun P K, Son D T and Starinets A O 2005 *Phys. Rev. Lett.* **94** 111601
- [13] Cao C, Elliott E, Wu H and Thomas J 2011 *New J. Phys.* **13** 075007
- [14] Adams A, Carr L D, Schäfer T, Steinberg P and Thomas J E 2012 *New J. Phys.* **14** 115009
- [15] Elliott E, Joseph J and Thomas J 2014 *Phys. Rev. Lett.* **113** 020406
- [16] Wang X, Li X, Arakelyan I and Thomas J 2022 *Phys. Rev. Lett.* **128** 090402
- [17] Pitaevskii L and Stringari S 2016 *Bose–Einstein Condensation and Superfluidity* Vol. 164 (Oxford University Press)
- [18] Shi Z, Li Z, Wang P, Han W, Huang L, Meng Z, Chen L and Zhang J 2023 *New J. Phys.* **25** 023032
- [19] Stringari S 1996 *Phys. Rev. Lett.* **77** 2360
- [20] Wang L, Yan X, Min J, Sun D, Xie X, Peng S G, Zhan M and Jiang K 2024 *Phys. Rev. Lett.* **132** 243403
- [21] Chen Q, Stajic J and Levin K 2005 *Phys. Rev. Lett.* **95** 260405
- [22] Elliott E, Joseph J and Thomas J 2014 *Phys. Rev. Lett.* **112** 040405
- [23] Hu H, Minguzzi A, Liu X J and Tosi M 2004 *Phys. Rev. Lett.* **93** 190403
- [24] Heiselberg H 2004 *Phys. Rev. Lett.* **93** 040402
- [25] Son D 2007 *Phys. Rev. Lett.* **98** 020604
- [26] Escobedo M A, Mannarelli M and Manuel C 2009 *Phys. Rev. A* **79** 063623
- [27] Dusling K and Schäfer T 2013 *Phys. Rev. Lett.* **111** 120603
- [28] Kinast J, Turlapov A and Thomas J E 2005 *Phys. Rev. Lett.* **94** 170404
- [29] Cao C, Elliott E, Joseph J, Wu H, Petricka J, Schäfer T and Thomas J E 2011 *Science* **331** 58
- [30] Bruun G M and Smith H 2007 *Phys. Rev. A* **75** 043612
- [31] Enns T, Haussmann R and Zwirger W 2011 *Annals of Physics* **326** 770
- [32] Nishida Y 2019 *Annals of Physics* **410** 167949
- [33] Hofmann J 2020 *Phys. Rev. A* **101** 013620
- [34] Kavoulakis G, Pethick C J and Smith H 1998 *Phys. Rev. A* **57** 2938
- [35] Yan X C, Sun D L, Wang L, Min J, Peng S G and Jiang K J 2021 *Chin. Phys. Lett.* **38** 056701
- [36] Yan X C, Sun D L, Wang L, Min J, Peng S G and Jiang K J 2022 *Chin. Phys. B* **31** 016701
- [37] Riedl S, Sánchez Guajardo E, Kohstall C, Altmeyer A, Wright M, Denschlag J H, Grimm R, Bruun G and Smith H 2008 *Phys. Rev. A* **78** 053609
- [38] Turlapov A, Kinast J, Clancy B, Luo L, Joseph J and Thomas J 2008 *Journal of Low Temperature Physics* **150** 567
- [39] Thomas J, Kinast J and Turlapov A 2005 *Phys. Rev. Lett.* **95** 120402
- [40] Ku M J, Sommer A T, Cheuk L W and Zwierlein M W 2012 *Science* **335** 563
- [41] Altmeyer A, Riedl S, Wright M, Kohstall C, Denschlag J H and Grimm R 2007 *Phys. Rev. A* **76** 033610
- [42] Kagamihara D and Ohashi Y 2017 *Journal of Low Temperature Physics* **187** 692